Available online at www.sciencedirect.com
ScienceDirect
Journal of Solid State Chemistry 181 (2008) 158–165
JOURNAL OF SOLID STATE CHEMISTRY
www.elsevier.com/locate/jssc

Synthesis, stoichiometry and thermal stability of Zn_3N_2 powders prepared by ammonolysis reactions

Giordano Paniconi[a], Zlatka Stoeva[a,1], Ronald I. Smith[b], Patricia C. Dippo[c], Bryan L. Gallagher[d], Duncan H. Gregory[e,*]

[a]*School of Chemistry, University of Nottingham, University Park, Nottingham NG7 2RD, UK*
[b]*ISIS Facility, Rutherford Appleton Laboratory, Chilton, Didcot OX11 0QX, UK*
[c]*Measurements and Characterization Division, National Renewable Energy Laboratory, 1617 Cole Boulevard, Golden, CO 80401, USA*
[d]*School of Physics and Astronomy, University of Nottingham, University Park, Nottingham NG7 2RD, UK*
[e]*Department of Chemistry, WestCHEM, Joseph Black Building, University of Glasgow, Glasgow G12 8QQ, UK*

Received 16 October 2007; accepted 1 November 2007
Available online 13 November 2007

Abstract

Zn_3N_2 powders were prepared by ammonolysis reactions at 600 °C and examined by thermogravimetric analysis, powder X-ray and neutron diffraction. The powders obtained in this way are unstable in an oxygen atmosphere above 450 °C. In an argon atmosphere, the powders are stable up to their decomposition point at around 700 °C. Structural models obtained from Rietveld refinements against the powder neutron diffraction data indicate that the Zn_3N_2 powders so-prepared have the *anti*-bixbyite structure and are almost certainly stoichiometric with no compelling evidence of nitrogen vacancies. Further, no evidence was found for aliovalent oxygen substitution at the nitrogen sites. The calculated bond valence sums imply that Zn_3N_2 cannot be described as a 100% ionic compound. The structural findings are supported by photoluminescence measurements that reveal a band gap of approximately 0.9 eV.

Keywords: Zinc nitride; Powder neutron diffraction; Stoichiometry; Nitrogen vacancies; Ammonolysis

1. Introduction

Zn_3N_2 is a group II–V semiconducting compound which is currently attracting significant research interest because of its promising electronic and photonic properties. Zn_3N_2 was first examined in 1940 by Juza et al. [1,2] who reported that this compound crystallises in the *anti*-bixbyite structural type. The precise crystal structure was later refined by Partin et al. [3] using time-of-flight (TOF) powder neutron diffraction (PND) data. In the cubic *anti*-bixbyite structure, the metal atoms are in tetrahedral sites of an approximately cubic close packed array of nitrogen atoms. The zinc atoms occupy general crystallographic positions whereas the nitrogen atoms occupy two different sites. The *anti*-bixbyite structure is adopted by several other nitrides, including Mg_3N_2, Be_3N_2 and Cd_3N_2 [1–3].

Zn_3N_2 can be synthesised by several methods, each of which yields products of differing morphologies. Juza et al. [2] reported the preparation of polycrystalline Zn_3N_2 either by the thermal decomposition of $Zn(NH_2)_2$ or via the ammoniation of zinc powder at 600 °C. More recently, Zong et al. [4] prepared Zn_3N_2 powder by a nitridation reaction of Zn powder with NH_3 gas at 600 °C for 120 min. Polycrystalline Zn_3N_2 and $Zn_xN_yO_z$ thin films can be obtained by reactive radio frequency magnetron sputtering [5,6] or by annealing zinc metal films in an NH_3 flow at 410 °C [7]. Furthermore, recently Zn_3N_2 was synthesised in other interesting and unusual morphologies, including nanowires [8] and empty balls [9].

Although Zn_3N_2 was first studied more than 60 years ago, details about its electronic and optical properties have emerged only recently. Futsuhara et al. [6] established that Zn_3N_2 obtained by magnetron sputtering is an *n*-type

*Corresponding author. Fax: +1 44 141 3304888.
E-mail address: D.Gregory@chem.gla.ac.uk (D.H. Gregory).
[1]Present address: Cambridge Enterprise, University of Cambridge, 10 Trumpington Street, Cambridge CB2 1QA, UK.

0022-4596/$ - see front matter © 2007 Elsevier Inc. All rights reserved.
doi:10.1016/j.jssc.2007.11.005

semiconductor with a direct band gap of 1.23 eV. The same authors also reported that the Zn_3N_2 films obtained in this way showed high electronic mobility of about $100\,cm^2\,V^{-1}\,s^{-1}$ at room temperature. Kuriyama et al. [7] on the other hand, found that Zn_3N_2 has a band gap of 3.2 eV. In the latter case, the Zn_3N_2 films were prepared by direct reaction between NH_3 and Zn layers evaporated on quartz substrates. Kuriyama et al. [7] proposed that the large band gap of Zn_3N_2, as compared to other II–V compounds, originates from the larger ionicity of the Zn–N bond. The value of the band gap for Zn_3N_2 remains debatable. Recently, changes in the band gap energy were attributed to unintentional doping due to oxygen contamination of Zn_3N_2 films grown by metalorganic chemical vapour deposition and radiofrequency molecular beam epitaxy [10].

In view of the applications of Zn_3N_2 and the contradictory reports of its electronic properties, it is of interest to examine the structure–property relations in more detail. Structural details are particularly relevant to the electronic and optical properties of Zn_3N_2: nitrogen vacancies and/or excess metal atoms lead to the generation of free electrons which determine the type of conduction, whereas the concentrations of free electrons (the charge carrier numbers) determine the levels of electronic conductance. Similarly, oxygen substitution at the nitrogen site is expected to influence the electronic properties and the optical band gap.

In this work, we have used PND to examine the stoichiometry of Zn_3N_2 powders prepared by ammoniation in terms of both nitrogen deficiency and oxygen substitution at the nitrogen site. Previously, these structural details have been deduced from X-ray measurements [17]. With the exception of the investigation carried out by Partin et al. [3], no neutron diffraction studies have been reported as yet. Moreover, the effect of the synthesis conditions on the crystal structure and the issue of stoichiometry in Zn_3N_2 were not examined in this previous neutron study [3]. In the present article, we describe our studies to establish the precise structural details for Zn_3N_2 and relate them to both the preparation conditions and the properties of the materials so produced.

2. Experimental

The Zn_3N_2 powders were synthesised by reacting Zn dust of particle size 5–10 μm (Aldrich, 98 + %) with NH_3 gas (BOC, purity 99.999%) at 600 °C. Examination of the Zn dust by X-ray diffraction (XRD) gave no evidence for the presence of crystalline impurity phases. The ammonia gas was additionally dried by passing through a bottle filled with CaO. The reactions were carried out in a Carbolite™ tube furnace fitted with a quartz reaction tube of length 70 cm and internal diameter 2.9 cm. In each reaction, 1.5–2.0 g zinc dust was placed in an alumina boat and transferred to the furnace where ammonia gas was passed over it at a flow rate 500–700 ml min^{-1}. All syntheses included initial preheating at 450 °C for 15 min under flowing ammonia followed by heating at 600 °C for specified reaction times. At the end of each reaction, the furnace was switched off and the products left to cool to ambient temperature in an inert atmosphere, by replacing the ammonia gas with argon (BOC, purity 99.9995%). After each reaction, some amount of zinc was found condensed on the inside surface of the quartz tube. This explains the relatively low yield from the ammonolysis reactions that varied between 60% and 65 wt% of the theoretical amount, according to

$$3Zn + 2NH_3 \rightarrow Zn_3N_2 + 3H_2. \quad (1)$$

The nitrogen content in the Zn_3N_2 samples was determined by elemental analysis using a CE440 elemental analyzer with a thermal conductivity detector from Exeter Analytical Ltd.

Thermogravimetric analysis (TGA) was carried out using a TA Instruments SDT-Q600 balance. TGA scans were carried out under oxygen and argon gas flows. The samples, typically 25–35 mg were contained in open alumina crucibles. In all cases, the heating rate was 5 °C/min from 25 to 1000 °C and the gas flow was 60 mL min^{-1}.

Phase purity was assessed from powder X-ray diffraction (PXD) data collected on a Philips XPERT θ–2θ diffractometer with monochromated Cu$K\alpha$ radiation ($\lambda = 1.5405$ Å). The 1-h scans over the range 10–80° 2θ were cross-referenced to powder patterns generated from the inorganic crystal structure database (ICSD) using Powdercell 3 [12]. As described later, the reaction products consisted of Zn_3N_2 as a main phase, in addition to small amounts of ZnO as an impurity phase. ZnO was always observed to be a by-product in this reaction, as noted by other authors [4,11]. We observed formation of ZnO regardless of the purity of the zinc powder staring material and even in cases where the ammonia gas was dried over two bottles filled with quicklime, CaO. (Conversely, reducing the purity of the ammonia from 99.999% to 99.99% led to phase fractions of ZnO larger by an order of magnitude; typically, ca. 60%.) An alternative potential source of oxygen was considered to be the alumina reaction boat and, indeed, the phase fraction of ZnO in the ammoniation products could be reduced—but not to <5 wt%—by vacuum drying the alumina crucible for 20–24 h before use. A similar phase fraction of ZnO was achieved using degassed BN boats. Further, quartz work tubes were observed to yield the highest phase fractions of nitride under the adopted experimental conditions (vs. e.g. alumina, mullite and steel).

Lattice parameters for the initial assessment of the crystal structure were obtained by indexing the powder patterns using DICVOL91 [13]. Rietveld refinements against PXD data were performed using the general structure analysis system (GSAS) [14]. Initial cycles refined the background coefficients and scale factors, followed by refinement of the lattice parameters. As the refinements progressed, peak width parameters, isotropic thermal

vibration parameters and site occupancy factors were varied. The refinements produced reasonable best-fit values and suggested that the anti-bixbyite structural model was correct. However, no reliable information could be obtained about the occupancies of the two nitrogen sites and possible oxygen substitution. In order to obtain more precise structural information, especially anion positions and content, PND experiments were carried out.

TOF PND data were collected using the POLARIS medium resolution diffractometer at the ISIS pulsed spallation source, Rutherford Appleton Laboratory, UK. The samples, 1–3, ca. 1.5–2 g each (Table 2), were loaded into 6 mm diameter thin-walled cylindrical vanadium cans and neutron diffraction data collected at room temperature. The crystal structures were refined using the GSAS [14] software package with data from all three detector banks simultaneously. Initial cycles of the refinements allowed for the variation of the scale factor, six background coefficients (modelling as a power series to account for increased contributions with rising Q; function type 4 within GSAS) and the lattice parameters. As the refinements progressed, atomic coordinates and thermal displacement parameters, peak width parameters and absorption coefficients were introduced. Peak shapes were modelled using a convolution of back-to-back exponentials with a pseudo-Voigt function (profile function 3 in GSAS). Finally, the site occupancy factors were allowed to vary and attempts were made to model any oxygen substitution at the nitrogen sites. In order to avoid unrealistic values, the thermal factors and the occupancies of the two nitrogen sites were constrained to be the same. At the final stages of the refinements, there was strong correlation between the occupancy factors and the thermal vibration parameters of the two nitrogen sites. Further details about the structural refinements and interpretation of the results are given in the Discussion section.

The Zn_3N_2 band gap was determined from room temperature photoluminescence (PL) measurements using an Oriel InstaSpec IV charged-coupled device (CCD) and a MS-257 imaging spectrograph. Data were acquired using InstaSpec software and corrected for system response. A Kimmon IK Series 442 nm He–Cd laser at 20 mW was utilised for excitation.

3. Results and discussion

3.1. Evolution of the Zn_3N_2 phase

Preliminary experiments and PXD examination of the reaction products showed that Zn_3N_2 is obtained after ammonolysis reactions at 600 °C for approximately 12 h. Under these experimental conditions, only a small amount of ZnO impurity could be detected. At shorter reaction times we observed significant amounts of unreacted zinc metal whereas longer reaction times resulted in the formation of ZnO. Complete oxidation to ZnO was found after 30 h. Elemental analysis confirmed that the maximum nitrogen content (10.91(5)%) was found for samples prepared for 12 h. XRD patterns for selected samples obtained during the preliminary investigation are illustrated in Fig. 1. The corresponding preparation conditions are listed in Table 1.

Previous reports indicate that single-phase Zn_3N_2 powders can only be obtained within limited temperature and time intervals [2,4,11]. Analysis of thermodynamic and kinetic data show that reduction of Zn_3N_2 in ammonia flow begins at very low ammonia dissociation levels, achievable at temperatures as low as 500–550 °C [15–18]. The reduction process (from N_2+H_2) leads to the formation of zinc metal that is highly reactive and easily interacts with traces of oxygen to form ZnO. Previous studies by other authors, as well as the results presented here show that prolonged heating at 600 °C under ammonia flow leads to the formation of ZnO [4,11,19]. We note that various reaction times are reported in the literature as being optimal for the preparation of Zn_3N_2. In each case, the optimum reaction time depends on the specific reaction conditions, including the use of quartz or

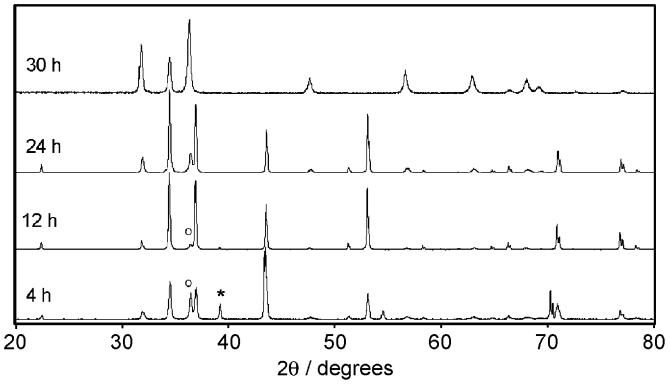

Fig. 1. Powder X-ray diffraction patterns for the products of the ammonolysis reactions at different reaction times (samples A–D as designated in Table 1). Reaction times are given next to each diffraction pattern. The symbols show characteristic reflections that can be used to identify the phases unambiguously. Star symbol (*) shows the strongest non-overlapping reflection for Zn metal, open circle (○) shows the reflections for ZnO.

Table 1
Preparation conditions and phase composition of the products of ammonolysis reactions at 600 °C for different reaction times (samples A–D)

Samples for X-ray	Synthetic conditions	Products	Nitrogen content (%)
A	600 °C, 4 h, quartz reaction tube	Zn, Zn_3N_2, ZnO	3.5
B	600 °C, 12 h, quartz reaction tube	Zn_3N_2, ZnO	10.91
C	600 °C, 24 h, quartz reaction tube	Zn_3N_2, ZnO	8.67
D	600 °C, 30 h, quartz reaction tube	ZnO	0

ceramic reaction tubes, the ammonia flow rate, particle sizes of the starting zinc powder, etc. These observations are not surprising considering the fact that ammonia dissociation itself depends strongly on such conditions. Original studies demonstrated that ammonia dissociates to a different degree according to the character and extent of the surface in contact with the gas as well as the material of the tube [17,18]. Hence, given the often subtle but, equally, often very significant effects of these many variables, it is particularly worth highlighting that being able to reproduce the synthesis and preparation of Zn_3N_2 is a most challenging task. All aspects of the synthesis need to be considered with great care.

3.2. Thermal stability

The thermal stability of the Zn_3N_2 powders depends on the working gas environment. As shown in Fig. 2a, Zn_3N_2 is stable in argon up to around 700 °C. The weight loss starts at 650 °C and becomes significant above 700 °C. This weight loss can be attributed to decomposition of the samples. The decomposition temperature found for Zn_3N_2 is lower than the boiling point of zinc metal that is 907 °C at atmospheric pressure.

Fig. 2b shows the TGA curves obtained in oxygen gas. In this case, the sample weight increases significantly above 450 °C which is attributable to oxidation of Zn_3N_2 according to

$$2Zn_3N_2 + 3O_2 \rightarrow 6ZnO + 2N_2. \quad (2)$$

The measured weight gain for samples 1–3 as listed in Table 2 is 7.71% for sample 1, 8.01% for sample 2 and 8.48% for sample 3. These values take into account the presence of ZnO impurity as found in the Rietveld refinements. The weight gain in all cases is lower than the theoretical value of 8.9% for full oxidation. These results suggest perhaps one of three things: (1) incomplete bulk oxidation which might be due to the short time of exposure to oxygen and the configuration of the TGA experiment. It is thus possible that only the surface of the nitride particles is oxidised whereas the centre of the particles still contains Zn_3N_2; (2) alternatively, it could be argued that the lower than expected weight gains imply the formation of single-phase oxynitride either pre- or post TGA oxidation. We are currently investigating this possibility in more detail but the former (i.e. that an oxynitride is the identity of 1, 2 or 3) is not indicated by PND; finally, (3) there is the possibility that the phase fraction of ZnO in the PND samples is underestimated in the refinements. This is distinctly plausible, especially if any oxide in 1–3 is amorphous or poorly crystalline.

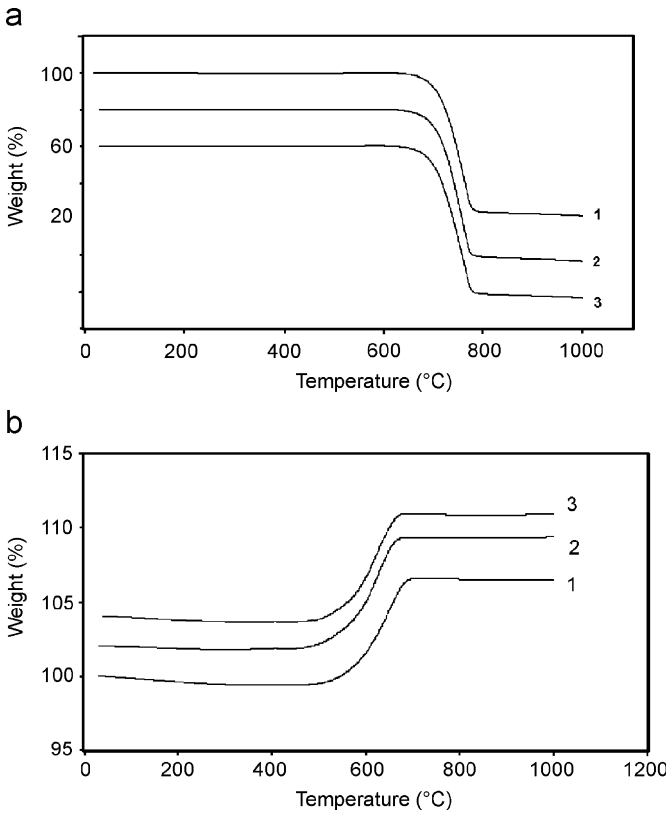

Fig. 2. Thermogravimetric analysis profiles for Zn_3N_2 samples 1–3 (a) in argon gas flow and (b) in oxygen gas flow. For clarity, the curves for samples 2 and 3 are displaced downwards by 20% and 40%, respectively, in (a) and upwards by 2% and 4%, respectively, in (b).

3.3. Crystal structure

Samples 1–3 were examined by PND. These samples had high Zn_3N_2 content, with a relatively amount of ZnO present as an impurity phase. Due to severe peak overlap, multi-phase samples containing Zn_3N_2, ZnO and unreacted Zn metal were not suitable for Rietveld refinement in the context of the present work. Refined structural data are listed in Tables 3 and 4. Representative fitted diffraction profiles after Rietveld refinement are illustrated in Fig. 4.

The crystal structure obtained in this work and illustrated in Fig. 3 compares well with the previous study by Partin et al. [3] performed on commercially sourced nitride. Notably, the quality of the TOF data from POLARIS have allowed us to determine crystallographic parameters with high precision. The nitrogen atoms form an approximately cubic close packed framework with the zinc atoms located in tetrahedral interstitial sites. The zinc atoms occupy one crystallographic site, the general position, 48*e*. The nitrogen atoms occupy two different crystallographic sites: N(1) at the 8*b* ($\frac{1}{4}$, $\frac{1}{4}$, $\frac{1}{4}$,) position and N(2) at the 24*d* (x, 0, $\frac{1}{4}$,) position (x∼0.978).

Table 2
Preparation conditions for the samples examined by powder neutron diffraction (1–3)

Sample no.	Synthetic conditions
1	600 °C, 11 h, quartz reaction tube
2	600 °C, 12 h, quartz reaction tube
3	600 °C, 13 h, quartz reaction tube

3.4. Stoichiometry in Zn_3N_2

As discussed in the introduction section, the nitrogen stoichiometry and possible aliovalent substitution by oxygen are very important for the electronic and optical properties of Zn_3N_2. Therefore, attention focussed on testing various structural models against the neutron diffraction data which are well suited for determining the population of the nitrogen sites. In the first model tested, the nitrogen occupancy was varied, initially constraining the occupancy fractions for the two nitrogen sites to be the same and subsequently varying them freely. The results of each strategy resulted in N site occupancies within 1 standard uncertainty (1σ) of unity. For samples 1 and 2, unconstrained refinement of the N1 and N2 site occupancies produced values between 0.96 and 0.99 for the N1 site and values of 1.0 for N2 with negligible change to the goodness-of-fit parameters and errors within 1σ of unity. Hence the overwhelming evidence was for models stoichiometric in nitrogen. At most, therefore, there is only the suggestion that these samples might exhibit a slight nitrogen deficiency at the N1 site. By contrast, the occupancy of both nitrogen sites for sample 3 tended to converge to values slightly above 1 (1.001–1.003), consistently within 1σ of unity. The occupancies of both N sites were thus fixed at one in the final refinement cycles for each of the samples 1–3. The final structural data are listed in Tables 3 and 4.

A second model assuming partial substitution of oxygen at the nitrogen sites was tested as an alternative to the anion-deficient models above. Given that simultaneous refinement of two anion occupancies and vacancies is not physically meaningful, the total anion occupancy of each nitrogen site was fixed at one. However, the introduction of mixed O/N occupancy at either or both of the two nitrogen sites neither led to physically meaningful anion occupancies, nor produced improvements in the goodness-of-fit parameters for any of the samples. The substitution of oxygen at the nitrogen sites is expected to reduce the lattice parameter, *a,* because of anticipated shorter Zn–O bond lengths. For example, Sakamoto et al. [11] reported *a*-parameters between 9.753 and 9.765 Å for the anion

Table 3
Crystallographic data for 1–3 from powder neutron diffraction data

Sample no.	1	2	3
Temperature of data collection (K)	295	295	295
Space group	$I\,a\,\bar{3}$	$I\,a\,\bar{3}$	$I\,a\,\bar{3}$
a-Parameter (Å)	9.77966(2)	9.77856(2)	9.77956(2)
Unit cell volume (Å)	935.342(1)	935.028(3)	935.315(3)
Density (g cm)	6.367	6.369	6.369
Weight fraction Zn_3N_2	0.929(1)	0.933(2)	0.903(2)
Weight fraction ZnO	0.071(1)	0.067(2)	0.097(2)
R_p	0.0445	0.0440	0.0452
WR_p	0.0266	0.0255	0.0267
χ^2	1.407	1.154	1.207

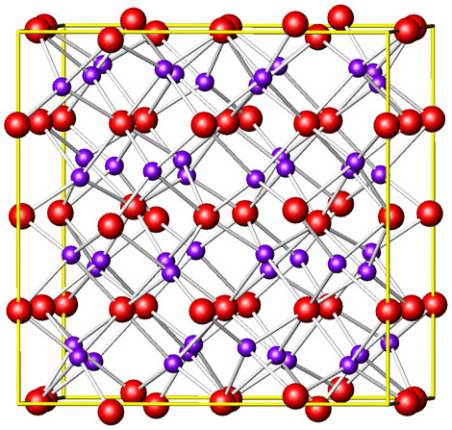

Fig. 3. Crystal structure of Zn_3N_2. Large red circles represent nitrogen atoms, small purple circles show the zinc atoms. The unit cell is outlined with yellow lines.

Table 4
Refined atomic positions and anisotropic displacement parameters for 1–3

	x	*y*	*z*	Occupancy	$100 \times U_{11}$, U_{22}, U_{33}, U_{12}, U_{13}, U_{23}/Å^2
Sample 1					
Zn	0.39658(5)	0.15071(5)	0.37509(4)	1	0.74(2), 0.79(2), 0.62(1),0.013(8), −0.26(1), −0.24(1)
N(1)	0.25	0.25	0.25	1	0.62(1), 0.62(1), 0.62(1),0.08(1), 0.08(1), 0.08(1)
N(2)	0.97826(2)	0	0.25	1	0.61(1), 0.56(1), 0.65(1), 0, 0, −0.03(1)
Sample 2					
Zn	0.39649(5)	0.15082(5)	0.37504(5)	1	0.80(2), 0.76(2), 0.58(1), 0.017(8), −0.26(1), −0.22(1)
N(1)	0.25	0.25	0.25	1	0.62(1), 0.62(1), 0.62(1), 0.11(1), 0.11(1), 0.11(1)
N(2)	0.97825(3)	0	0.25	1	0.64(1), 0.55(1), 0.61(2), 0, 0, 0.002(11)
Sample 3					
Zn	0.39652(5)	0.15075(6)	0.37504(5)	1	0.72(2), 0.77(2), 0.59(1), 0.014(8), −0.27(1), −0.22(1)
N(1)	0.25	0.25	0.25	1	0.62(1), 0.62(1), 0.62(1), 0.08(1), 0.08(1), 0.08(1)
N(2)	0.97825(3)	0	0.25	1	0.61(1), 0.56(1), 0.62(2), 0, 0, −0.03(1)

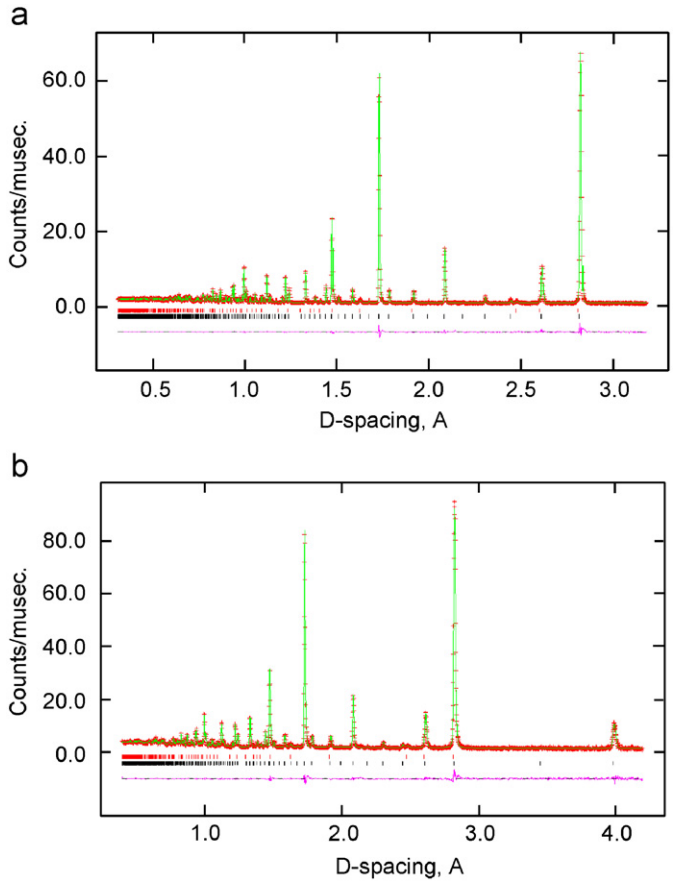

Fig. 4. Profile fits for sample 2 following Rietveld refinement (a) backscattering detector bank ($\langle 2\theta \rangle = 145°$) and (b) 90° detector bank ($\langle 2\theta \rangle = 90°$). Crosses show the observed data points, solid lines represent the calculated diffraction patterns, black vertical bars represent the calculated reflection positions for Zn_3N_2, red vertical bars represent calculated reflection positions for ZnO.

deficient oxynitrides $Zn_3(N_{1-x}O_x)_{2-y}$. The *a*-parameter found in our work shows essentially no dependence on the synthetic conditions and is larger than the *a*-parameters found in the oxynitride samples reported in Ref. [11]. The results from the structure refinements described here in combination with the band gap data presented below hence signify that these materials are nitrides rather than oxynitrides.

3.5. Bonding in Zn_3N_2

The four Zn–N bond lengths are not all equal but vary between 2.01 and 2.27 Å as listed in Table 5. The Zn–N bond lengths in Zn_3N_2 are slightly longer than those found in $ZnGeN_2$, a compound which contains Zn in similar tetrahedral coordination with Zn–N bond lengths between 2.00 and 2.02 Å [20]. In Zn_3N_2, the Zn–N bond lengths are much longer than those in A_2ZnN_2 (A = Ca, Sr, Ba), a group of nitrides which contain linear nitridometallate anions $[N = Zn = N]^{4-}$ [21,22]. Zn–N distances in such linear geometry vary between 1.8418 Å for Ca_2ZnN_2 and 1.874 Å for Sr_2ZnN_2. On the basis of bond length–bond strength arguments, the longer Zn–N bonds in Zn_3N_2 are a reflection of the increased coordination number over that in A_2ZnN_2, but the increase in distance may also suggest less π-character to the Zn–N bonds in Zn_3N_2.

Table 5
Selected bond lengths for Zn_3N_2 for 1–3

	Sample 1	2	3
a-Parameter/Å	9.77966(2)	9.77856(2)	9.77956(2)
Zn–N(1)/Å	2.1200(6)	2.1185(6)	2.1191(6)
Zn–N(2)/Å	2.2667(3)	2.2667(4)	2.2668(4)
Zn–N(2)/Å	2.0057(4)	2.0058(4)	2.0061(4)
Zn–N(2)/Å	2.0754(5)	2.0758(6)	2.0755(6)
Zn–Znx2/Å	2.7086(7)	2.7070(7)	2.7075(7)
Zn–Znx2/Å	2.7429(7)	2.7440(8)	2.7438(8)
Zn–Znx2/Å	3.1647(2)	3.1643(2)	3.1648(2)

Table 6
Bond valence sums for each site in Zn_3N_2 for 1–3

Sample	V [Zn]	V [N(1)]	V[N(2)]
1	1.62	2.33	2.46
2	1.62	2.34	2.46
3	1.62	2.34	2.46

Bond valence sums at the atoms in Zn_3N_2 were calculated using the method developed by Brown [23] and Brese and O'Keeffe [24]. This approach makes use of the fact that the bond length is a unique function of bond valence, hence, it provides empirical tools for the interpretation of bond lengths found experimentally. In this case, the bond valence parameter $R_{ZnN} = 1.77$ Å was taken from Ref. [24]. The bond lengths and fractional occupancies were obtained from the structure refinements as described above. The calculated bond valence sums are listed in Table 6 and we use these values as a premise for a semi-quantitative description of the chemical bonding in Zn_3N_2. All bond valence values are smaller than the values for ideal ionic Zn_3N_2, i.e. 2 for Zn and 3 for nitrogen. Our results agree very well with the values reported by Partin et al. [3]. The same authors argued that the low bond valence sums for Zn_3N_2 and the isostructural *anti*-bixbyite Mg_3N_2 are a manifestation of nonbonding metal–metal interactions. The shortest Zn–Zn distances in Zn_3N_2 from our data (2.71 Å) are 1.5% longer than those in metallic zinc (2.67 Å) [25].

3.6. Band gap measurements

Results from room temperature PL measurements are illustrated in Fig. 5. The spectra show broad peaks centred at around 0.85–0.90 eV, with no significant difference in onset between the three samples. Comparison with previous reports shows that this is one of the smallest

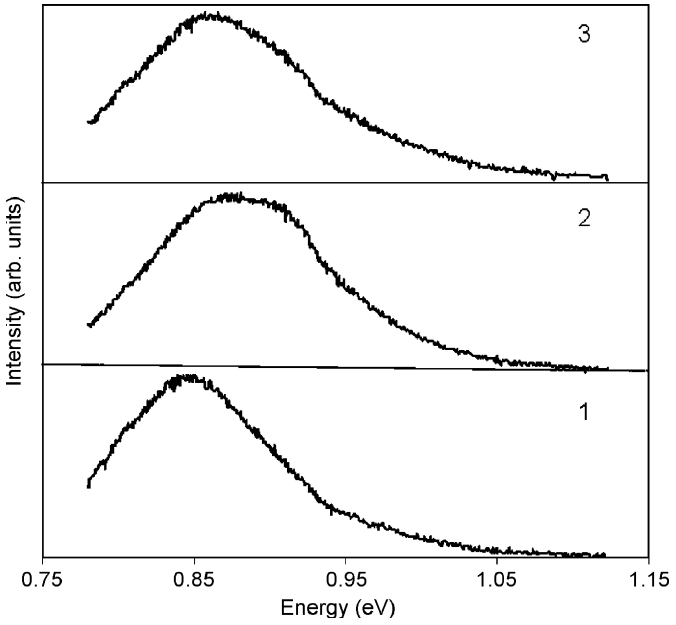

Fig. 5. Room temperature photoluminescence spectra for samples 1–3.

band gaps reported for Zn_3N_2. Our values from PL measurements, however, are in broad agreement with a recent systematic study of Zn_3N_2 polycrystalline films which found that the actual band gap—extracted from optical and carrier concentration measurements—is 1.06 eV [10]. In the general case, the band gap for Zn_3N_2 increases if oxygen is introduced into the lattice because of the high ionicity of the Zn–O bond (i.e. increased electronegativity of O over N). The results presented here demonstrate that the Zn_3N_2 samples under investigation are unlikely to contain oxygen within the lattice (and hence that the samples are not bulk oxynitrides) and corroborate our PND structural models.

3.7. Discussion

From the published literature reports, it is clear that the band gap and other electronic properties of Zn_3N_2 are intimately related to the stoichiometry and composition of the material. Oxygen substitution (i.e. the formation of oxynitrides) leads to increasing ionic character and correspondingly, an increased band gap [5,10]. Additionally, oxygen substitution increases the carrier concentration and affects the electronic mobility. If control cannot be exerted over the stoichiometry of Zn_3N_2, then erroneous and contradictory band gap and electronic conductivity data may result, which are key parameters for material properties and applications.

The data amassed in this study indicate that the Zn_3N_2 samples are all nitrides as opposed to oxynitrides and likely to be fully stoichiometric. PND data strongly suggest that any possible nitrogen deficiency is likely to be negligible in the bulk materials (and only exist in 1 and 2). It might be argued that were any appreciable concentration of nitrogen vacancies to be present, these would decrease with longer reaction times. Further, one might argue that were substitutional or interstitial oxide to become a significant phenomenon, then this would become more prevalent with increased reaction time. In fact, under the conditions of our experiments, prolonging the duration of the reaction merely produces more phase-separated ZnO (hence decreasing the phase fraction of a Zn_3N_2 phase otherwise indistinguishable from those in samples prepared over shorter periods). That any possible differences in the nitrogen stoichiometry between the three bulk samples are probably negligible is echoed in the PL data where the effect on the emission is also small. A recent DFT study investigated the possible pathways for O incorporation within Zn_3N_2, both via substitutional and interstitial mechanisms and revealed that the former was the lower energy process [26]. Such considerations could be very important in the production of Zn_3N_2 films, but our results strongly demonstrate that powdered samples prepared via careful ammonolysis methods do not undergo such substitutional processes in the bulk, even with some variation in processing parameters.

Sub-stoichiometric nitrides of the groups IV and V transition metals crystallising in the rock salt structure, such as TiN_x and VN_x, are well documented [27]. The nitrogen vacancies in these cases induce the formation of new bonding states between the metals surrounding the vacancy that results in significant changes of the physical, thermodynamic and mechanical properties. However, the existence and role of nitrogen vacancies in nitrides with the *anti*-bixbyite structure is neither well documented nor well understood. Further studies are highly desirable in view of the potential applications of these compounds, not least of Zn_3N_2 itself as one of the most promising members of this structural group. It is highly likely that important modifications to the electronic structure can be made as much by judicious changes to the surface structure/composition and particle size/morphology as by manipulating the bulk. This is an area that clearly requires much further investigation.

4. Conclusions

Zn_3N_2 powders were prepared by ammonolysis reactions and examined by TGA, PXD and PND. Structural studies indicate that Zn_3N_2 synthesised in this way contains no oxygen in the bulk and is almost certainly stoichiometric. Room temperature PL measurements yield a band gap of 0.85–0.9 eV, commensurate with materials that do not contain oxygen as oxynitride.

Acknowledgments

DHG and BLG thank the University of Nottingham (under the IDTC for photonics and electronics) for a studentship to G.P. The CCLRC (UK) is gratefully

acknowledged for the award of beam time at ISIS, Rutherford Appleton Laboratory, UK.

References

[1] R. Juza, H. Hahn, Z. Annorg. Allg. Chem. 244 (1940) 125.
[2] R. Juza, H. Hahn, Z. Annorg. Allg. Chem. 244 (1940) 133.
[3] D.E. Partin, D.J. Williams, M. O'Keefe, J. Solid State Chem. 132 (1997) 56.
[4] F. Zong, H. Ma, C. Xue, H. Zhuang, X. Zhang, H. Xiao, J. Ma, F. Ji, Solid State Commun. 132 (2004) 521.
[5] M. Futsuhara, K. Yoshioka, O. Takai, Thin Solid Films 317 (1998) 322.
[6] M. Futsuhara, K. Yoshioka, O. Takai, Thin Solid Films 322 (1998) 274.
[7] K. Kuriyama, Y. Takahashi, F. Sunohara, Phys. Rev. B 48 (1993) 2781.
[8] F. Zong, H. Ma, J. Ma, C. Xue, X. Zhang, H. Xiao, F. Ji, H. Zhuang, Mater. Lett. 59 (2005) 2643.
[9] F. Zong, H. Ma, C. Xue, W. Du, X. Zhang, H. Xiao, J. Ma, F. Ji, Mater. Lett. 60 (2006) 905.
[10] T. Suda, K. Kakishita, J. Appl. Phys. 99 (2006) 076101.
[11] T. Sakamoto, R. Saki, T. Moriga, K.I. Murai, I. Nakabayashi, Int. J. Mod. Phys. B 17 (8–9) (2003) 1523.
[12] G. Nolze, W. Kraus, Powder Diffr. 13 (1998) 256.
[13] A. Boultif, D. Louer, J. Appl. Crystallogr. 24 (1991) 987.
[14] A.C. Larson, R.B. von Dreele, The General Structure Analysis System, Los Alamos National Laboratories, Report LAUR 086–748; LANL:Los Alamos, NM, 2000.
[15] A.M. Zykov, F.F. Grekov, D.M. Demidov, Z. Prikl. Khim. 44 (8) (1971) 1700.
[16] M.D. Lyutaya, S.A. Bakuta, Poroshk. Metall. 2 (206) (1980) 57.
[17] A.H. White, W. Melville, J. Am. Chem. Soc. 27 (1905) 373.
[18] W. Ramsay, S. Young, J. Chem. Soc. Trans. 45 (1884) 88.
[19] F. Zong, H. Ma, C. Xue, H. Zhuang, X. Zhang, J. Ma, F. Ji, H. Xiao, Sci. China Ser. G 48 (2) (2005) 201.
[20] M. Wintenberger, M. Maunaye, Mater. Res. Bull. 8 (1973) 1049.
[21] M.Y. Chern, F.J. DiSalvo, J. Solid State Chem. 88 (1990) 528.
[22] H. Yamane, F.J. DiSalvo, J. Solid State Chem. 119 (1995) 375.
[23] I.D. Brown, Structure and Bonding in Crystals, Vol. 2, M. O'Keeffe, A. Navrotsky (Eds.), Academic Press, New York.
[24] N.E. Brese, M. O'Keeffe, Acta Crystallogr. B 47 (1991) 192.
[25] A.W. Hull, W.P. Davey, Phys. Rev. 17 (1921) 549.
[26] R. Long, Y. Dai, L. Yu, M. Guo, B. Huang, J. Phys. Chem. B 111 (2007) 3379.
[27] L.E. Toth, Transition Metal Carbides and Nitrides, Academic Press, London, 1971.